Geophysical Journal International

Geophys. J. Int. (2013) **193,** 252–262 doi: 10.1093/gji/ggs082

Mechanical healing of simulated fault gouge

Y. H. Messen,[1,*] A. Corfdir[1] and J. Schmittbuhl[2]

[1] *Université Paris-Est, Laboratoire Navier (UMR 8205), CNRS, ENPC, IFSTTAR,* F-77455 *Marne-la-Vallée, France. E-mail: ymessen@hotmail.com*
[2] *Institut de Physique du Globe de Strasbourg, Université de Strasbourg/CNRS,* 5 *rue René Descartes,* 67084 *Strasbourg, Cedex, France*

Accepted 2012 November 21. Received 2012 November 20; in original form 2011 December 12

SUMMARY

We investigate the origin of fast shear strength healing induced by mechanical perturbations during slide-release-slide (SRS) experiments using a ring shear apparatus (ACSA, Navier/CERMES, Ecole des Ponts ParisTech, France). A 100-mm-thick annular sample of siliceous sand (0.6 mm mean diameter) is submitted to shear by the mean of a rotating cylinder in a semi-Couette geometry. We explore the role of shear stress perturbations related to small reverse offsets of the loading interface. We show that controlled releases of the shear stress induce shear strength increases when resuming shear load (i.e. the Tightening-up effect of unloading or Tu-effect). However, a threshold of the shear stress perturbation amplitude to get a significant restrengthening is observed. The shear strength increase is shown to be logarithmically related to the amount of imposed reverse offset and linearly to the induced volumetric strain. These results suggest that small perturbations of the contact status (i.e. inelastic strain) in the granular assembly of the gouge interface, have a major influence on the fault restrengthening.

Key words: Creep and deformation; Fracture and flow; Friction; Rheology and friction of fault zones; Dynamics and mechanics of faulting.

1 INTRODUCTION

Mechanical responses of faults are generally described by friction constitutive laws which are classically expressed in terms of slip, sliding rate and state of shear zone (Scholz 1992). One of the most studied and used law is the rate and state friction (RSF) law (Dieterich 1979b; Ruina 1983). Classical RSF laws account for the effect of stationary contact conditions (Karner & Marone 1998), as shown by laboratory experiments where the friction strength of simulated faults increases with time of contact or with decreasing slip rate (Dieterich 1979a; Beeler *et al.* 1994). This evidence, associated with field observations, indicates that fault will strengthen during the interseismic period following a time-dependent healing (Li *et al.* 1983; Scholz 1992; Beeler *et al.* 1994; Karner *et al.* 1995; Marone *et al.* 1995; Tadokoro & Ando 2002; Nakatani & Scholz 2004). Besides time-dependent effects, other parameters affect faults healing: velocity-strengthening (e.g. Mair & Marone 1999), hydrothermal and chemical healing (Olsen *et al.* 1998; Nakatani & Scholz 2004; Yashuhara *et al.* 2005) and normal stress variation healing (Linker & Dieterich 1992; Richardson & Marone 1999). Interestingly, most of these studies do not consider shear stress as a possible factor affecting friction strength (Nakatani 1998). So several questions arise: what role do shear stress perturbations play on sliding friction? Does exist a mechanical healing due to shear stress perturbations? If shear stress release effects exist, are they time-dependent? Actually several authors (Nakatani & Mochizuki 1996; Karner & Marone 1998, 2001; Nakatani 1998; Olsen *et al.* 1998) have investigated the effects of shear stress perturbations and holds on the frictional behaviour of fault surfaces. Indeed, they run different types of slide-hold-slide (SHS) experiments in which holds are preceded by rapid reduction of the shear stress. Using double-direct shear apparatus with bare surfaces, Nakatani & Mochizuki (1996) found a composed effect: a time-dependent increase in static friction and a time-independent increase in dynamic friction caused by lowering shear stress; the latter was called the 'Tightening-up effect of unloading (Tu effect)'. They underlined that this effect is more important in magnitude than time- and slip-rate-dependent effects described by RSF laws. They also observed an important effect in this strengthening played by the gouge which was produced during the abrasion of the initially bare surfaces. Nakatani (1998) was interested in studying closely the 'Tu effect' on surfaces separated by a thin gouge layer; he found a linear relationship between time-independent strengthening and shear stress reduction. Without measuring the variation of layer thickness but based on literature studies, he attributes the strengthening to the consolidation of the gouge. He also attributes the slip weakening following this healing to the gouge unconsolidation. Karner & Marone (2001) brought out the significant difference between shearing within granular materials and shearing of bare surfaces. They investigate under a wider range the effects of the shear load, hold time, loading rate and initial layer thickness on frictional healing using double-direct shear

∗ Now at SYSTRA, 72 rue Henry Farman, 75513 Paris Cedex 15, France.

apparatus. They found, among other observations, that healing and compaction increase with shear load reduction. Furthermore, large perturbations of normal or shear load far from steady state are not well described by existing friction laws (Karner & Marone 1998, 2001). Other devices, notably ring shear apparatus, were used to study friction behaviour by Tullis & Weeks (1986), Beeler *et al.* (1996), Tika (1999), Clausen & Gabrielsen (2002), Garga & Sendano (2002) and Agung *et al.* (2004). In these experiments, rotary tests are conducted either on soil samples or on rock blocks with or without thin gouge layer. While most of the investigations were conducted with the double-direct shear apparatus or ring shear apparatus (or also with triaxial apparatus) on rock blocks separated or not by a thin (at the most 3 mm) gouge layer, Chambon *et al.* (2006a) carried out tests on the Cylinder Shear Apparatus (ACSA; Corfdir *et al.* 2004) in which shear stress is applied by mean of a rotating cylinder surrounded by a thick sample (100 mm) of granular material (semi-Couette geometry). This is an interesting feature for considering large thickness of fault gouge (Chambon *et al.* 2006c). Indeed Karner & Marone (2001) showed that the healing effect is stronger for thick sample. Another advantage of ACSA is the large possible shear displacement with a homogeneous applied shear slip on the whole sliding surface with no loss of material. Chambon *et al.* (2006a) actually observed significant restrengthening after each shear sense reversal during which the shear stress was fully released.

To further investigate the first observations made by Chambon *et al.* (2006a), this paper presents an extended experimental study of the frictional healing induced by shear stress releases using the same ACSA setup. Our experiments have been carried out on a simulated fault gouge made of dry dense sand. Experiments are of the type: slide-release-slide (SRS) test. First slip is imposed at a constant rate. Then, after a given slip distance, shear stress is rapidly reduced to a prescribed value by imposing to the cylinder a small reverse offset in the reverse direction, and then slip is resumed at the prior direction and rate. No significant time-dependent processes were observed and we studied healing as a function of shear stress release (obtained by small reverse offset of the loading interface). Results show systematic shear strength healing after release events; a perturbation threshold is highlighted under which no restrengthening is observed. Furthermore, an instantaneous compaction/dilatancy attached to each perturbation event indicates a correlation between volumetric strain and healing strength.

2 EXPERIMENTAL SETUP

2.1 Apparatus description

Experiments were performed with the ACSA (Fig. 1). We only present here this apparatus shortly. More detailed information can be obtained from Lerat (1996) and Corfdir *et al.* (2004). The apparatus consists of a cylinder surrounded by a thick annular sample (Fig. 2), with a height and a width of 0.1 m. The inner radius of the sample is $R_i = 0.1$ m, and the outer radius is $R_e = 0.2$ m.

Fig. 3 shows the boundary conditions of the sample. By mean of a rotating cylinder the inner side of the sample is submitted to an imposed displacement at a constant rate. The outer side is separated from water confinement by a neoprene jacket of 2 mm thick. Water is contained in a cell (Fig. 1) and connected to a pressure/volume controller (max. press: 2 MPa, vol.: 10^{-3} m^3, resolution: 1 kPa and 1 mm^3, accuracy <0.25 per cent). This controller ensures a constant radial stress σ_e (up to 1 MPa). A vertical stress σ_v is applied by the

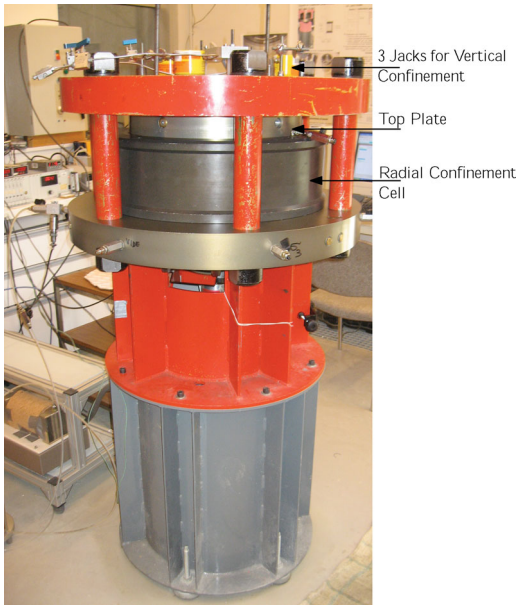

Figure 1. View of the Cylinder Shear Apparatus (ACSA).

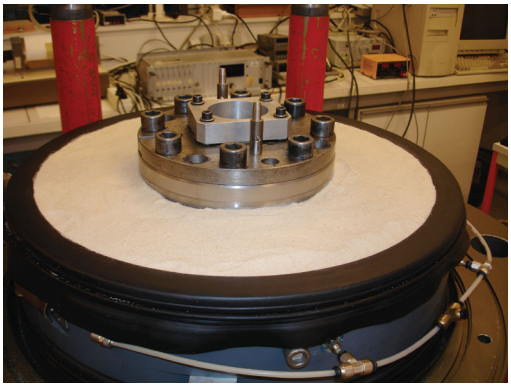

Figure 2. View of an open cell with the sand sample surrounding the metallic cylinder.

mean of three jacks through a top plate made of aluminum alloy (Fig. 1); the jacks are connected to a pressure/volume controller (max. press: 64 MPa, vol.: 2.10^{-4} m^3, resolution: 1 kPa and 1 mm^3, accuracy <0.1 per cent). Verticals displacements of the top plate are measured with three LVDTs (30 mm length, 0.3 per cent accuracy). In our experiments, vertical displacements (towards the top) were prevented; compaction was still possible but did not happen in our experiments. The bottom plate under the sample is interchangeable and made of glass or stainless steel. It is immobile during test.

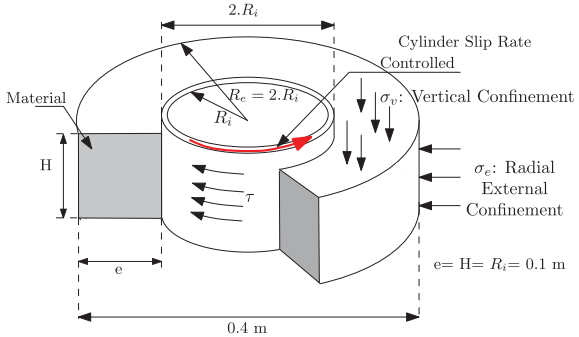

Figure 3. Sample dimensions and boundary conditions.

We used in our experiments a rough inner cylinder made in Dural (density of 2.8 10^3 kg m^{-3}, E = 73 GPa and $\nu = 0.3$). Its roughness is made of triangular grooves perpendicular to the sliding direction. The grooves are 0.7 mm deep and 2 mm apart. With this setup, shearing can be applied at a prescribed rate between 1.7 and 100 μm s^{-1} but we adopted in this study a constant rate of 83.3 10^{-6} m s^{-1}.

The main limitation of the ACSA in comparison with the conventional geophysical experimental studies is the applied load level. Indeed the maximum radial confining pressure is 1 MPa. In our experiments, we adopted a confining pressure of 0.5 MPa.

2.2 Measured parameters

The rotation angle φ of the cylinder is measured with a 15-bit optical encoder providing a 0.011° resolution. The corresponding tangential displacement δ at the inner boundary of the sample is deducted as $\delta = \varphi.R_i$ and is measured with a resolution of 1.92 10^{-5} m. The applied torque necessary to maintain the prescribed rate is measured by a torquemeter of 20 N.m accuracy. The average shear stress (τ) applied to the interface is estimated from:

$$\tau = \frac{\Gamma}{2\pi R_i^2 H}, \quad (1)$$

where Γ denotes the torque, H is the height of the interface (0.1 m) and R_i is the inner radius (0.1 m). Volumetric changes ΔV are deduced from a volume/pressure controller that monitors the radial confining pressure σ_e. ΔV corresponds to the variation of the amount of water contained in the confinement cell. Volumetric strain ε_v is calculated by dividing ΔV by the initial volume of the sample (9.42 10^{-3} m^3). Confining pressure is measured by a pressure sensor of 2 MPa range (<0.05 per cent BSFL accuracy). Sampling rate of measurements is 0.5 Hz.

2.3 Sample material

Experiments were conducted on angular Hostun siliceous sand (0.4/0.8 mm) with grain density of about 2.65. Fig. 4 shows the grain-size distribution of this sand and Table 1 gives its chemical composition. Experiments were carried out at room temperature and hygrometric conditions.

The choice of a quasi-mono-disperse granular material (sand) is motivated by a fast and reproducible preparation of samples. Real fault gouges are made of cataclastic rocks with a large grain size

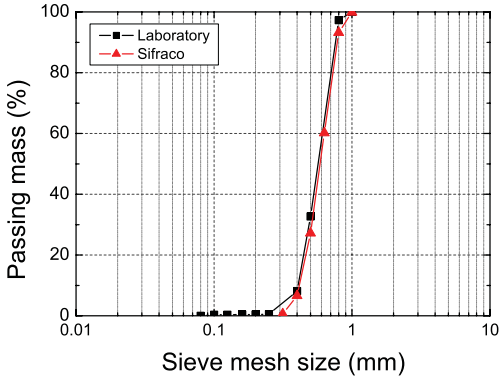

Figure 4. Grain-size distribution of the Hostun (HN; 0.4/0.8) sand from supplier data (SIFRACO) and our own laboratory check with a laser granulometer.

Table 1. Chemical composition of Hostun HN 0.4/0.8 sand (Supplier: SIFRACO).

Silica ($Si0_2$)	>99.0 per cent
Iron oxide (Fe_20_3)	<0.1 per cent
Alumina (Al_2O_3)	<0.4 per cent
Potassium oxide (K_2O)	<0.2 per cent
Calcium oxide (CaO)	<0.1 per cent

distribution and a significant cohesion (Chester & Chester 1998; Scholz 2003; Chester *et al.* 2004; Chambon *et al.* 2006a). Despite its simplification, the use of sand in our experiments still takes into account some important characteristics of natural fault gouge like granularity, angular grains submitted to attrition (Chambon *et al.* 2006a). Numerous studies have also adopted granular material, typically quartz sands or glass beads with diameters at a wide range from 0.05 to 0.5 mm as a proxy of fault gouge (e.g. Olsen *et al.* 1998; Géminard *et al.* 1999; Karner 2006).

The sand particles were deposited in successive layers of 0.02 m. Each layer was gently compacted to reach a dense state with a total density ranging from 1.60 10^3 to 1.64 10^3 kg m^{-3}. The confining pressure is then applied. Before starting test, the sample is let for several hours during which it compacts. The corresponding volumetric variation during this phase is monitored by the volume/pressure controller.

3 EXPERIMENTAL PROCEDURE

3.1 Stress release technique

In our experiments, the gouge layer was sheared at a reference slip rate maintained constant at 83.3 10^{-6} m s^{-1}. Then, at a given displacement (every 1 m) shear stress is rapidly released from τ_{pr} until a target value τ_r (Fig. 5a). Shear load release was obtained by imposing a small reverse offset of hundreds of microns in the reverse rotation direction (Fig. 5b). Once target shear stress is reached at $\tau_r \pm 10$ per cent, shearing is resumed in the initial direction. To analyse the results, we define in Fig. 5(a) the healing strength by $\Delta\tau_h = \tau_p - \tau_{pr}$ and the relative magnitude of the shear stress perturbation, or release level, by $R = \Delta\tau_r/\tau_{pr} = (\tau_{pr} - \tau_r)/\tau_{pr}$. For large shear release, reloading triggers an increase of shear strength up to a peak τ_p before a subsequent slip-weakening. Fig. 5(a) shows two release events corresponding to a complete release ($R = 100$ per cent) and a partial release ($R = 85$ per cent). Fig. 5(b) is a close-up of the first release sequence after $\delta_c = 2$ m cumulative slip; it shows the loop followed by shear stress as a function of displacement and defines the reverse offset $\Delta\delta_c$.

3.2 Experimental programme

Four tests were performed on initially new sample. Each experiment was conducted following a release plan that defines the value of release level R_i at the corresponding cumulative displacement δ_i. Table 2 presents experiment features: initial state of the sample, background shear rate (before shear release and at resuming), release rate and confining pressure. Table 3 indicates the adopted release plans for each test. Test CR006 dealt with the three smallest values of R while other tests were performed at higher levels: $R > 60$ per cent. To minimize the effect of material state change and sand comminution on healing, releases were applied following plans respecting antidrift design sequences (Goupy 1993).

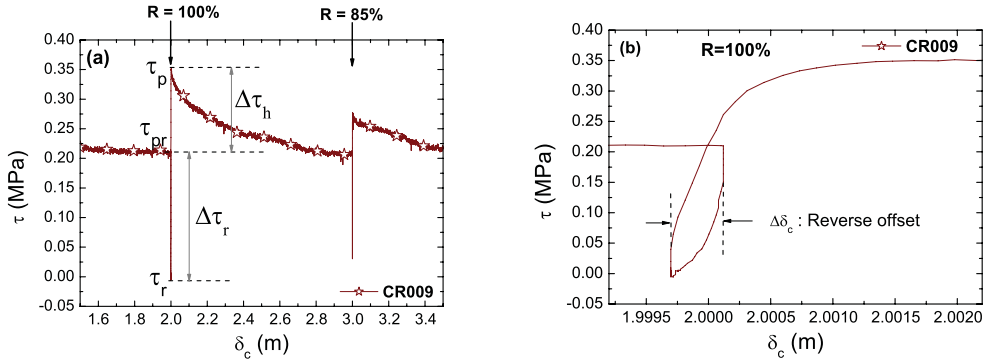

Figure 5. (a) Shear stress variation during slip (δ_c) showing two release sequences at 2 and 3 m with R equal to 100 per cent and 85 per cent, respectively; it also indicates definition of the different parameters used in data analysis, $\Delta\tau_r$ is the released amount of shear stress while $\Delta\tau_h$ represents the strengthening. (b) Close-up of the release sequence at $\delta_c = 2$ m with $R = 100$ per cent. It shows the loop followed by shear stress as a function of the displacement defining the reverse offset $\Delta\delta_c$ necessary to reach the target release level R.

Table 2. Experiments summary.

Test	Sand	Shear rate (10^{-6} m s^{-1})	Release rate (10^{-3} MPa/s)	Confining pressure σ_e (MPa)
CR003	New	83.3	−0.6 to −1	0.5
CR005	New	83.3	−3.6 to −5	0.5
CR006	New	83.3	−3.6 to −5	0.5
CR009	New	83.3	−3.6 to −5	0.5

Furthermore, CR009 test was conducted following three phases. The first one (0–5 m) consists of release sequences similar to that of the other tests. The subsequent phases (6–9 m) and (10–14 m) include the repetition of the same release plan. Note that the 85 per cent release during Phase 2 was not done.

4 RESULTS

4.1 Reproducibility of the shear stress response

Fig. 6 shows shear stress variations for tests CR003 and CR005 during which the sample is submitted to shear stress reduction of different magnitudes. At experiment start (after 3 to 4 · 10^{-3} m), shear stress increases up to a peak of 0.590 MPa which is followed by a large slip weakening of about 60 per cent in magnitude, as previously observed by Chambon *et al.* (2006a). Then after each stress perturbation, shear stress increases at reloading up to a new peak but typically smaller than the initial phase. We observe a large restrengthening for large shear releases, with a long slip to reach back the pre-release level. Our aim here is to study the effect of the shear stress release magnitude and rate on this healing strength.

The two experiments, CR003 and CR005, were conducted at exactly the same conditions in terms of: confining pressure, sample density, background slip rate (before shear release and at resuming) and release plan (see Tables 2 and 3), except the release rate. Indeed, we adopted a different unloading rate for the CR003 test: it was six times slower than for CR005 and the rest of tests (see Table 2). Otherwise, the loading shear rate is maintained constant and equal to 83.3 10^{-6} m s^{-1}.

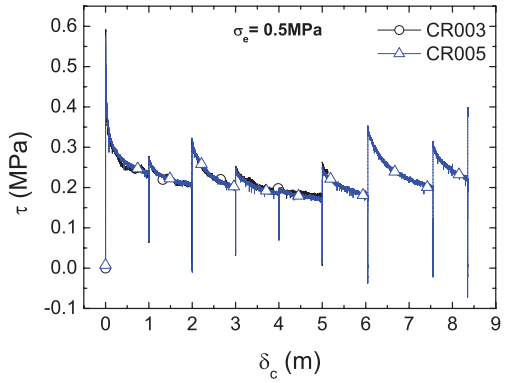

Figure 6. Shear stress (τ) variation in function of cumulative displacement (δ_c) involving different releases as indicated by Table 3. Considered tests: CR003 (○) and CR005 (△) conducted under 0.5 MPa confinement. Release rate was six times slower for CR003 (see Table 2); in spite of this fact, the shear stress curve is identical to that of CR005 indicating a remarkable reproducibility and no time effect.

Fig. 6 shows a perfect reproducibility in terms of shear stress variation both at restrengthening (peaks) and during slow slip weakening. This result suggests that there is no time effect, at least for the 'hold' periods used in our tests. Karner & Marone (2001) noted a negligible effect of unloading rate consistently with our observations. Nakatani (1998) argued that the frictional healing caused by shear stress decrease was far greater than that produced by rate variation. By conducting shear rate variation and hold sequences, Chambon *et al.* (2006b) also indicated that the effect of these two parameters on the shear strength is a second-order process compared to the effect induced by the mechanical perturbation. All these observations make the observed time-independent mechanical healing consistent with the results of Nakatani (1998).

Table 3. Values of the target release level R (in per cent) for each test and cumulative displacement δ_c.

	δ_c (m)	1	2	3	4	5	6	7	8	9	10	11	12	13	14
Test	CR003	71	100	84	60	96	-	-	-	-	-	-	-	-	-
	CR005	72	100	83	62	94	121	111	133	-	-	-	-	-	-
	CR006	30	96	54	6	75	-	-	-	-	-	-	-	-	-
	CR009	73	100	85	66	94	77	102	65	93	75	105	85	68	93

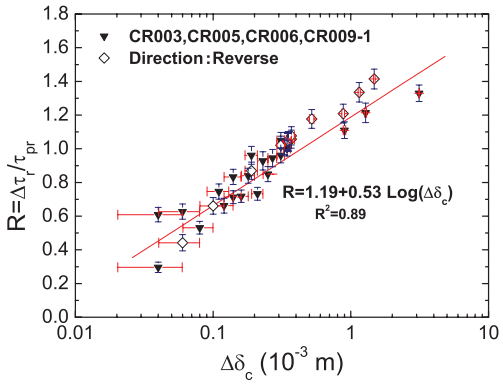

Figure 7. Semi-logarithmic plot of shear stress release level R versus imposed reverse offset $\Delta\delta_c$ (in mm): (▼) CR003, CR005, CR006 and Phase 1 of CR009 and (◇) for a reverse direction (Direction: Reverse, in the legend) of a separate test. The red line is a logarithmic fit: $R = 1.19 + 0.53\ \log(\Delta\delta_c)$.

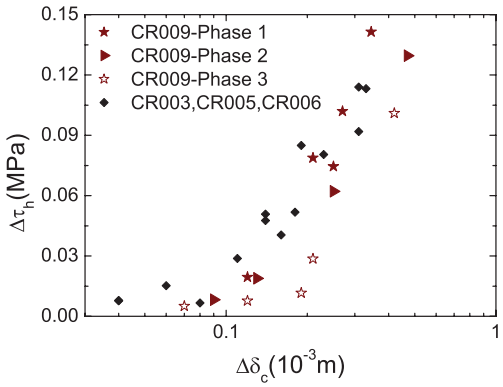

Figure 8. Semi-logarithmic plot of healing strength $\Delta\tau_h$ versus reverse offset $\Delta\delta_c$. Note the reduction of healing with slip from phase to phase and the shift to the left of the data squatter, especially for Phase 3. Data acquisition for the three phases of CR009 [Phase 1: (★), Phase 2: (▶) and Phase 3: (☆)], are compared to the other tests (CR003, CR005, CR006) with (♦) symbols.

4.2 Shear stress release versus imposed reverse offset

We indicated in Section 3.1 that to decrease shear stress, a small displacement $\Delta\delta_c$ in the reverse direction, that is, a reverse offset, is necessary. To illustrate the relationship between shear stress perturbation and reverse offset, Fig. 7 shows the relative magnitude of the shear stress perturbation, or release level, $R = \Delta\tau_r/\tau_{pr}$ as a function of the reverse offset amplitude $\Delta\delta_c$ in a semi-logarithm diagram. A clear linear trend over two orders of magnitude in reverse offset, indicates that at first order, the shear release level R is a logarithmic function of the reverse offset $\Delta\delta_c$: $R \propto \log(\Delta\delta_c)$. Note that no reverse offset was recorded (at least at the encoder resolution) for small releases ($R < 30$ per cent).

Karner & Marone (2001) have also observed a reverse slip during the hold period of their SHS experiments for high releases. They attribute this slip to compaction and time-dependent decay of elastic strain within the gouge layer. They proposed that this phenomenon has a small effect on healing. It is of interest to see that Nakatani & Scholz (2004), who induced shear stress perturbations and not reverse offset, obtained also rather long effective D_c (of the order a millimetre) although they attributed the origin to time effects which is different from this study. A common effect could be however that the bulk around the interface has been modified suggesting that any mechanism that induce a significant perturbation of the bulk leads to a long relaxation (or long D_c).

4.3 Healing strength versus imposed reverse offset

Magnitude of healing strength is quantified by the relative amplitude of the shear stress peak when load is resumed: $\Delta\tau_h$. Fig. 8 shows $\Delta\tau_h$ as a function of the reverse offset $\Delta\delta_c$. In our tests, healing is initiated when reverse offset is larger than a threshold of the order of 0.1 mm which can be compared to a fraction of the grain size. The threshold corresponds to a relative stress release of $R \approx 60$ per cent. Above the threshold of 0.1 mm ($R \approx 60$ per cent), shear strength healing evolves logarithmically with the reverse offset amplitude: $\Delta\tau_h \propto \log(\Delta\delta_c)$.

4.4 Volumetric strain response

Fig. 9(a) shows the volumetric strain evolution recorded during CR003 and CR005 tests. Shear stress variation was shown in Fig. 6. We first observe a long-term compaction which reaches nearly 1 per cent for the CR005 test. At the test beginning (close-up of Fig. 9 a), the sample is affected by a 0.05–0.07 per cent compaction over 1 to $1.8 \cdot 10^{-3}$ m. Then, it dilates by 0.18–0.21 per cent after 5 to 9 10^{-3} m of cumulative displacement. It compacts again gradually with displacement until the first shear perturbation at $\delta_c = 1$ m. A large amount of volumetric strain is undergone during the first metre of displacement. The slope of the curve decreases from step to step; each step is defined by a release followed by 1 m of slip. The reproducibility of the volumetric strain response is not as good as that of the shear stress (Fig. 6). During shear stress perturbation, a significant compaction is observed but rapidly followed by a short dilatancy period (of smaller magnitude than the compaction) and then a continuous slow compaction develops (see Fig. 9b which is a zoom of the volumetric strain response around the third and fourth releases of CR005, $R = 83$ per cent and $R = 62$ per cent, respectively). The same figure defines the parameters used in this study, namely the volumetric compaction at unloading: $\Delta\varepsilon_c = \varepsilon_{pr} - \varepsilon_r$ and the dilatancy at reloading: $\Delta\varepsilon_d = \varepsilon_p - \varepsilon_r$. Karner & Marone (2001) also observed that gouge layer dilates at reloading and that the dilatancy amount increases with the imposed unloading.

Fig. 10 shows a linear proportionality between the compaction $\Delta\varepsilon_c$ at unloading and the following dilatancy $\Delta\varepsilon_d$ at slip resuming (reloading). $\Delta\varepsilon_c$ increases with a slope of about 0.4. Note that the compaction amplitude $\Delta\varepsilon_c$ is greater than that of the dilatancy $\Delta\varepsilon_d$ which is consistent with Karner & Marone (2001) observations.

The relationship between the induced healing strength $\Delta\tau_h$ and the volumetric compaction $\Delta\varepsilon_c$ is illustrated in Fig. 11 which represents healing strength versus compaction volumetric strain for several experiments. This figure indicates clearly a linear trend between healing strength and compaction during shear stress release that passes through the origin. The link between these two parameters (healing strength and volumetric strain) have been studied in other configurations: for example, SHS tests in a double direct shear apparatus (Richardson & Marone 1999). Sleep *et al.* (2000) proposed to model the latter experiment on the basis of a single layer plastic model where plasticity is described by an RSF law. They showed that the plastic behaviour explains the linear relation between compaction and healing but also obtained that localization induces a bilinear relationship : at short hold time, the response is controlled by the localized shear band and at long time, a second linear relation emerges where the response is dominated by

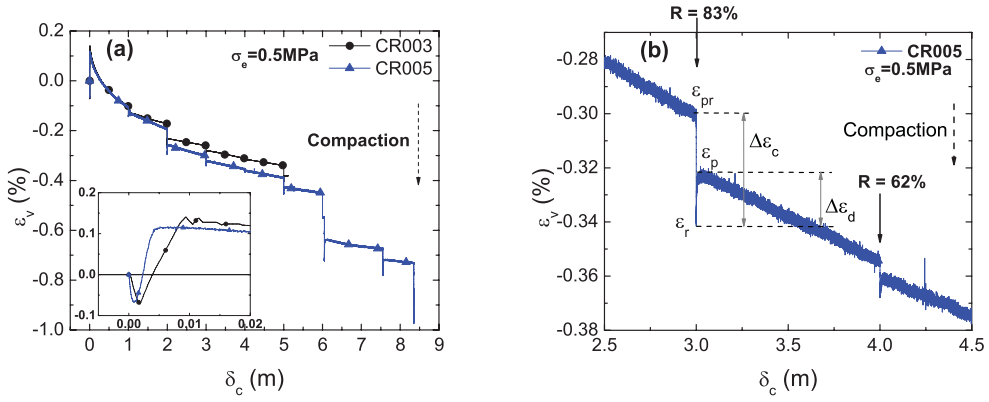

Figure 9. (a) Volumetric strain variation as a function of the cumulative displacement of CR003 (●) and CR005 (▲) tests. ε_v is equal to the volume change divided by the initial sample volume (9.425 10^{-3} m^3). A positive strain indicates dilatancy while a negative strain corresponds to compaction. A zoomed-in of the first centimetres is shown at the left bottom corner. (b) Definition of the different parameters used for data analysis. Close-up of CR005 data at 83 per cent and 62 per cent releases, respectively. $\Delta\varepsilon_c$ is the compaction during shear release and $\Delta\varepsilon_d$ is the dilatancy during reloading, that is, restart of the initial slip rate. ε_{pr} is the volumetric strain undergone just before the release.

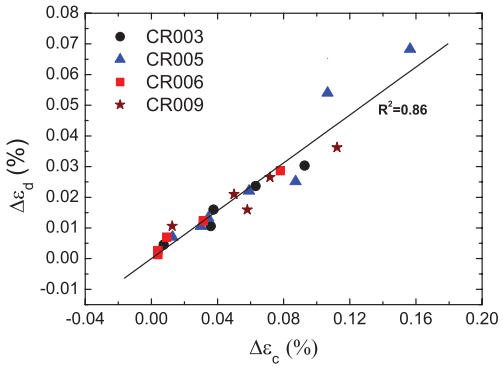

Figure 10. Volumetric dilatancy at reloading $\Delta\varepsilon_d$ as a function of the volumetric compaction during shear stress release $\Delta\varepsilon_c$. Black line fits the data of CR003 (●), CR005 (▲), CR006 (■) and first phase of CR009 (★).

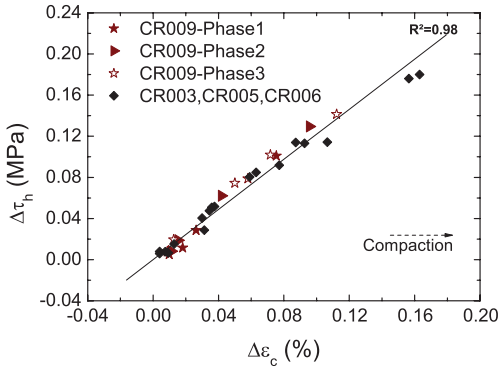

Figure 11. Healing strength $\Delta\tau_h$ as a function of the volumetric compaction during shear stress release $\Delta\varepsilon_c$. We interestingly observe no maturing effect related to large slip. Data come from the three phases of CR009 [Phase 1: (★), Phase 2: (▶) and Phase 3: (☆)], compared to the other tests (CR003, CR005, CR006) with (◆) symbols.

the whole sample. In our experiment, we do not see the dual behaviour but only a linear relationship of the first type (that passes through the origin) although strain localization definitely happened: the shear band being 5-mm-thick in a 100 mm sample. This comparison suggests that physical processes are different from Sleep's model (Sleep 1997). We rather consider that there exists an evolving coupling between the interfacial layer and the surrounding sample

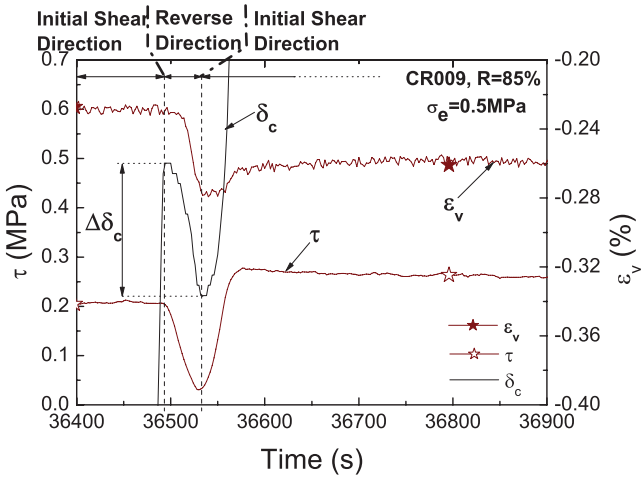

Figure 12. Detail of data acquisition at the third release sequence (R = 85 per cent) of CR009 illustrating the shear stress (☆) response measured by the torquemeter and volumetric strain (★) recorded by the volume/pressure controller (which measures the total sample volume across the confinement water variation), after 3 m of cumulative slip δ_c (line). Displacement is measured by the cylinder rotation encoder, and corresponds to the displacement at the interface steel/sample. The reverse offset undergone for the 85 per cent release is about 0.34 10^{-3} m.

that undergoes a slow compaction which makes it denser as in a secondary compression (Chambon *et al.* 2003, 2006a).

To illustrate the time relation between slip, shear stress and volumetric strain, Fig. 12 shows data from CR009 test in which shear stress is released by 85 per cent, by imposing a reverse offset $\Delta\delta_c$ of 0.34 10^{-3} m. This figure shows shear stress variation (open stars), volumetric strain (solid stars) and slip (solid line) all as a function of time, during the third release sequence conducted after 3 m cumulative slip δ_c. During reverse offset, shear stress immediately decreases together with a significant compaction after a slight delay. As soon as slip is resumed to the initial direction, shear stress rapidly increases and the sample dilates after a similar short delay. This slight delay of volumetric strain with respect to shear stress variation is that of the total sample which includes the volumetric strain of the interface and of the surrounding sample. Indeed the volume variation is measured at the outer boundary of the sample. Accordingly, the delay could be the signature of the time for

the dilatancy of the interface to overcome the slow compaction of the surrounding sample. We finally note that the rate of dilatancy decreases after the peak of shear stress.

5 DISCUSSION

5.1 Comparison with other works

Karner & Marone (1998, 2001) conducted conventional and modified SHS experiments using double-direct shear apparatus on granular quartz layers (50–150 μm size) sheared between solid forcing blocks at normal stress of 15 and 25 MPa. Holds were preceded by a rapid decrease of the shear load which is maintained until the end of the hold sequence. At resuming they observed that friction initially increases to a peak before evolving to a steady-state sliding. This is consistent with our observations (see Fig. 6). Lowering of shear stress was conducted for different values of η (i.e. the normalized shear stress at hold $\tau_{\rm hold}$ by the pre-hold shear stress $\tau_{\rm slide}$; η ranges from 0 to 1 and is equivalent to $(1-R)$ in our study). Karner & Marone (1998, 2001) found that frictional healing $\Delta\mu$, defined as the difference between peak and steady-state friction, decreases linearly with η. Nakatani & Mochizuki (1996) conducted the same type of experiments but on bare granite surfaces under 5 MPa of normal stress. They noted a time-independent increase in dynamic friction caused by lowering of the shear stress. They also underlined the important role that the gouge layer produced by friction of the initially bare surfaces plays.

Nakatani (1998) realized SHS experiments on thin gouge layer of crushed granite powder (<115 grit) sandwiched between two rough surfaces in a granite block. He also observed a significant restrengthening $\Delta\mu$ following shear stress release. He separated $\Delta\mu$ in two parameters: an instantaneous time-independent strengthening P2 and a time-dependent strengthening P1. The latter is present only for very low unloading. The healing strength $\Delta\mu$ was shown to decrease linearly with the ratio of the shear stress at hold and the normal stress ($\tau_{\rm hold}/\sigma$).

To compare our results with these references, Fig. 13 shows the healing strength $\Delta\tau_h$ normalized by the pre-release shear stress $\tau_{\rm pr}$ as a function of $\eta = \tau_{\rm r}/\tau_{\rm pr}$. To estimate $\Delta\tau_h$ from Nakatani (1998) results, we considered the two relationships that he established between P2 and $\tau_{\rm hold}$ on one hand, and P2 and $(\mu_* - \tau_{\rm hold}/\sigma)$ on the other hand, where $\tau_{\rm hold}$ represents the shear stress reached prior to hold, μ_* is the residual friction and σ the normal stress. We introduced a linear fit of the data with a slope of −0.22. For Karner & Marone (2001) results, we considered tests conducted on a 3-mm-thick initial layer, a constant rate and a normal stress of 25 MPa; the pre-release shear stress $\tau_{\rm pr}$ was taken as an average of 16.25 MPa (estimated as $\mu_{\rm pr}.\sigma$ with $\mu_{\rm pr} \approx 0.65$). We adopt a linear fit to their data where the slope is equal to −0.06. Finally, the linear fit of our data (CR003, CR005, CR006 and Phase 1 of CR009) gives a slope of −1.24.

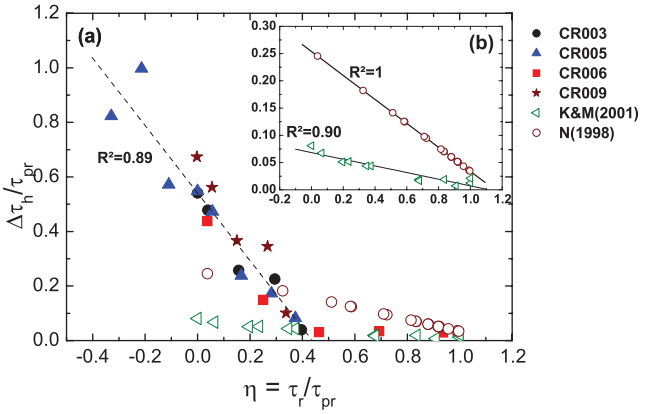

Figure 13. (a) Healing strength $\Delta\tau_h$ normalized by pre-release shear stress $\tau_{\rm pr}$ as a function of $\eta = \tau_{\rm r}/\tau_{\rm pr}$ defined by Karner & Marone (1998, 2001). Our data [CR003 (●), CR005 (▲), CR006 (■) and Phase 1 of CR009 (★)] compared to Nakatani (1998) results (○) under 5 MPa and 10 MPa of normal stress σ_n (fig. 6 of his article); and Karner & Marone (2001) results (◁) where $\sigma_n = 25$ MPa (fig. 7 of their article). Negative values of η relative to CR005 are reported to present releases larger than 100 per cent. Inset (b): Close-up of Nakatani (1998) and Karner & Marone (2001) data, where a linear fit is presented.

As shown in Fig. 13, a qualitative agreement could be mentioned between our results and that of the cited references: a linear decrease of the healing strength with the shear stress release both being normalized by the pre-perturbation shear stress magnitude. However, this plot shows a different slope for each data set. This could be attributed to the effect of the normal stress. We observe that the normalized healing strength ($\Delta\tau_{\rm r}/\tau_{\rm pr}$) and the slope, decrease with larger normal stress. Karner & Marone (2001), Nakatani (1998) and us, conducted tests under 25 MPa, 5–10 MPa and 0.5 MPa, respectively. Note that for $\eta = 1$, no release is imposed, despite a small restrengthening observed for the compared studies. This is due to the 100 s hold that these authors imposed systematically after each release. Another feature is the existence of a threshold in our experiments (Fig. 15a) for $\eta = 0.40$ ($R = 60$ per cent). Karner & Marone (2001) also pointed out a minimum of shear load reduction ($\eta = 0.90$) below which healing is low, an observation consistent with Olsen *et al.* (1998).

To compare volumetric strain of our experiments to layer thickness variation of Karner & Marone (2001), we considered the sample thickness reduction Δe during unloading (obtained in our experiments from the volumetric strain which is interpreted as a variation of the external radius of the sample) normalized by the thickness of the shear band e_0. This band is estimated to be seven grains thick (Chambon *et al.* 2006c) with grains of 0.6 mm, so $e_0 = 4.2$ mm. The same thickness of seven grains was considered for Karner & Marone (2001) where the grain size average is about 0.1 mm, so $e_0 = 0.7$ mm. Fig. 14 indicates a linear variation of $\Delta e/e_0$ with η both for our data and that of Karner & Marone (2001). When normalized to the seven-grains shear band thickness, unloading-induced

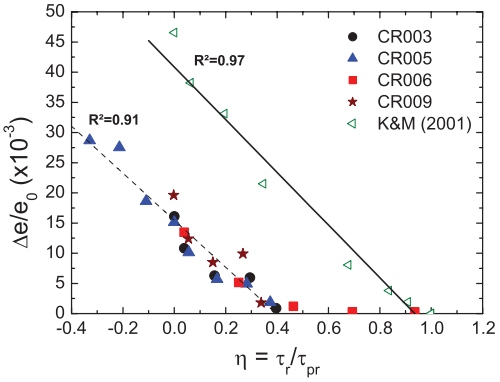

Figure 14. Variation of gouge layer thickness Δe (compaction) at slip perturbation normalized to shear interface thickness e_0 in function of $\eta = \tau_{\rm r}/\tau_{\rm pr}$ [CR003 (●), CR005 (▲), CR006 (■) and Phase 1 of CR009 (★)], compared to Karner & Marone (2001) data (◁) (fig. 7b of their article). e_0 considered is estimated according to Chambon *et al.* (2006b) of about seven grains [4.2 mm for our tests and 0.7 mm for Karner & Marone (2001).

compaction of Karner & Marone (2001) and the present experiments show a similar extent of linear dependence on the shear stress reduction (Fig. 14). However, when normalized to the total thickness of the sample, compaction of the present experiment is much less than KM2001. It seems like short-term compaction is more active within the shear band than in the bulk. Nakatani's (1998) results were not included since he did not record thickness variation.

Another kind of stress perturbation has been performed by Richardson & Marone (1999). These authors carried out normal stress variation (by a step or by vibrations) during holds of SHS experiments using double-direct shear apparatus on blocks separated by 3-mm-thick gouge layer of fine-grained quartz powder. The results show frictional relaxation and subsequent healing induced by stress variation which are greater compared to that enhanced by holds. They also show porosity decrease accompanying normal stress variation. The authors relate the normal stress-dependent healing to increased gouge compaction and alteration of the shear bands. These observations are consistent with our results of shear stress-induced healing since we highlight the important role of volumetric compaction which seems to be the preponderant factor leading to strength healing.

Interesting to note that Richardson & Marone (1999) also tried to model the frictional healing induced by vibrational SHS tests by the mean of the friction Dieterich and Ruina laws. This modelling was not able to adequately reproduce the observed results because of the inability to take into account the important gouge thickness effects.

5.2 Origin of shear strength weakening

Nakatani (1998) attributed the weakening that follows the restrengthening to gouge unconsolidation due to dilatancy or porosity increase. This conclusion is not consistent with our observations where the long-term weakening is accompanied by continuous compaction (Fig. 9a). As shown in this figure, the dilatancy phase is only present for the first 10 mm of displacement following the resuming of sliding. Chambon *et al.* (2006a) attributed the shear strength weakening over very large (1 m or even more) displacement, as observed in the case of the ACSA, to the progressive mechanical decoupling between the shear band and the bulk. In the latter study, the bulk of the sample, outside of the shear band, was shown to undergo a very slow compaction which was not negligible after very large slip. Moreover, from Correlation Imaging Velocimetry (CIV), the shear band was shown to not dilate during the slow compaction of the bulk of the sample which is consistent with the critical state of the shear band (with the ACSA setup, the displacement to reach the critical state is of the order of 4 mm). Consequently, the response at large slip is dominated by the response of the bulk rather than that of the highly sheared shear zone. This explanation contrasts with comminution-induced slip weakening theory (e.g. Marone *et al.* 1990; Beeler *et al.* 1996), in which the slip weakening is attributed to grain comminution and slow sample compaction. Nakatani (1998) also observed that the displacement required to erase healing induced by shear stress release was up to 2 mm. It is also conditioned by the thickness of the gouge layer: thicker samples need more sliding to erase completely the strengthening. In our experiments the sample was 100 mm thick. The sliding necessary to erase the strengthening depends also on its magnitude, and accordingly on the amplitude of the imposed shear stress perturbation. Moreover, no significant slip weakening was observed with double-direct shear tests on bare rock surfaces.

5.3 Maturing effects for large slip

We now discuss whether the mechanical healing remains reproducible for large shear displacement. In other words, does the gouge state play a role in this phenomenon? To address this question, we need to consider possible coupling between the effects of cumulative displacement, slip rate, shear or normal load perturbation, etc. In the case of our experiments, shear perturbations (related to reverse offset) are applied on a sample with an evolving material state owing to grain attrition, spatially inhomogeneous cohesion, bulk compaction, etc. This state evolution results from cumulative slip, slip perturbation and shear stress release. Chambon *et al.* (2006a) noted that the magnitude of shear stress peaks decreases with cumulative displacement of very large magnitude which indicates an effect of the sample history on restrengthening. Furthermore, Karner & Marone (2001) indicated that the frictional response following hold periods, was strongly dependent on the sample slip history. They also found that frictional healing and sliding friction decreased strongly with increasing slip (fig. 8b of their article). They finally observed that layer thickness variations are smaller for large total displacement. Moreover, Nakatani & Mochizuki (1996) who conducted experiments on initially bare granite surfaces indicate that the tightening-up effect was observed only for tests where the produced gouge was not removed from the sliding surface. This also indicates that the role played by the presence of gouge on the healing process, is important. Both cited references have conducted

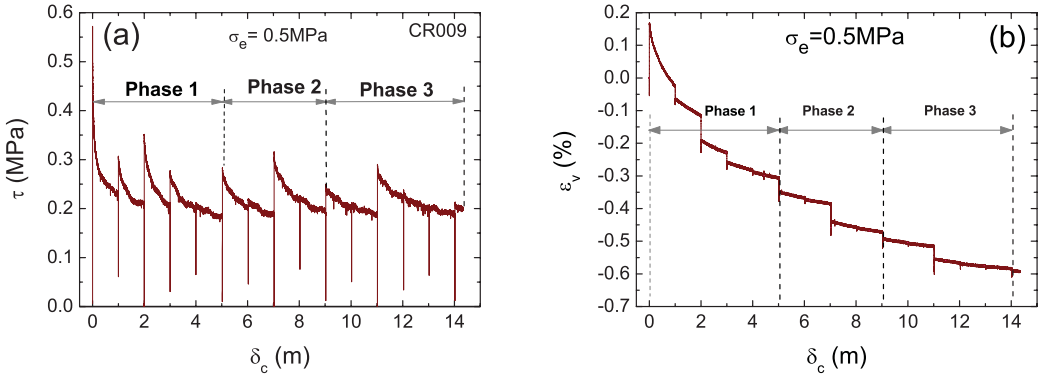

Figure 15. Data of CR009 test under 0.5 MPa confinement. (a) Shear stress τ, (b) volumetric strain ε_v. Three phases are distinguished: Phase 1 over 5 m slip, Phase 2 until 9 m cumulative slip and Phase 3 until 14.3 m cumulative displacement. Phase 2 contains four releases contrary to Phases 1 and 3 where five similar releases are conducted (see Table 3).

experiments with a small cumulative displacement, typically about 20–40 mm, limiting the role of the slip history on the mechanical healing process.

We tested the maturing effect during CR009 test. It was performed over more than 14 m of slip reproducing three times the same sequence of shear stress perturbations (see Fig. 15 and Table 3): Phases 1 to 3 (Phase 2 has a sequence of only four stress perturbations and lacks for the 85 per cent release). Each shear stress release was introduced after 1 m of slip. The confinement was maintained equal to 0.5 MPa. Measurements of shear stress and volumetric strain during this test are shown in Figs 15(a) and (b), respectively. The shear stress curve shows a global progressive reduction of the restrengthening from Phase 1 to Phase 3, even if shear stress perturbations are of the same order. The same trend is also observed in the case of volumetric strain, where the magnitude of the instantaneous deformation decreases with slip.

Fig. 8 shows healing strength $\Delta\tau_h$ versus reverse offset perturbation $\Delta\delta_c$ for each phase (solid stars for Phase 1, solid triangles for Phase 2 and open stars for Phase 3). These data are also compared to that of: CR003, CR005 and CR006, all indicated with solid diamond symbols. We observe a slight but significant shift of the shear strength increase $\Delta\tau_h$ with reverse offset $\Delta\delta_c$ from phase to phase, indicating reduction of $\Delta\tau_h$ for the same reverse offset $\Delta\delta_c$. Closer look at Fig. 8 shows that the minimum threshold of $\Delta\delta_c$ necessary for recognizable healing increases as more cumulative displacement is undergone, though the shift is limited within a range of 0.07–0.2 10^{-3} m for the tested range of cumulative displacement up to 14 m. The same behaviour is shown for the volumetric strain $\Delta\varepsilon_c$ in Fig. 16. For example, the compaction recorded for $\Delta\delta_c = 0.2\ 10^{-3}$m of Phase 3 of CROO9 is smaller than for the preceding phases.

Interestingly, Fig. 11 shows that the linear relationship between $\Delta\tau_h$ to $\Delta\varepsilon_c$, is not affected by the cumulative slip. Consequently, large slip clearly affects healing strength $\Delta\tau_h$ after each perturbation, by a reduction proportional to the decrease of the volumetric deformation $\Delta\varepsilon_c$. This result emphasizes the decisive role of volumetric deformation on shear strength healing.

5.4 Rapid and slow strain evolution

Fig. 17 shows volumetric strain evolution during CR005 test. The curve with solid triangles displays the total volumetric strain, and

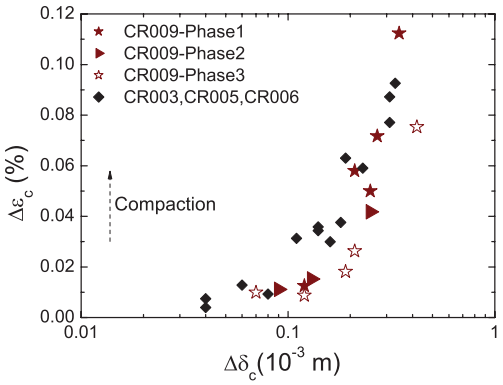

Figure 16. Semi-logarithmic plot of volumetric compaction $\Delta\tau_h$, versus reverse offset $\Delta\delta_c$. Note the reduction of compaction with slip from phase to phase and the shift to the left of the data squatter, especially for Phase 3. Data acquisition for the three phases of CR009 [Phase 1: (★), Phase 2: (▶) and Phase 3: (☆)], compared to the other tests (CR003, CR005, CR006) with (◆) symbols.

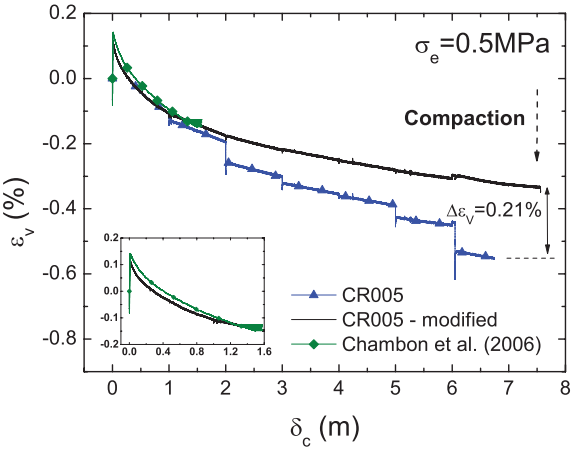

Figure 17. Volumetric strain of test CR005: the curve with solid triangles (▲) represents the recorded data and the curve with solid line represents the modified data corrected for perturbation-induced volumetric strain. Curve with solid diamond (◆) represents the data of Chambon (2003) recorded during the first phase of shearing over 1.6 m slip, a close-up is shown in the left bottom corner of this figure.

the solid line represents the total volumetric strain minus the perturbation-induced compaction/dilatancy during each shear stress perturbation. To compare with the volumetric strain undergone by shearing without shear stress perturbation, we added to the figure, Chambon *et al.* (2006a) data for a non-perturbed shear phase of 1.6 m slip (see IS phase of their fig. 7). We observe that the long-term compaction follows continuous long-term evolution, except for the offset due to the difference between unloading-induced compaction and loading-induced dilation. Unfortunately the volume variations are measured in the ACSA device using water volume variation of the outer confining cell. So the measure is a global estimate of volumetric strain and do not allow for a separation of the interfacial layer strain from that of the surrounding bulk.

The long-term compaction has also been observed in the case of glass beads for which no comminution or attrition occurred. Accordingly compaction is mainly due to particle rearrangement and not to grain comminution or attrition (Chambon *et al.* 2006a). According to these authors, the slow compaction takes place in the bulk of the sample, outside of the interfacial layer which rapidly reaches its critical state (Marone & Scholz 1989). It can also be noted that the shear band is a small part of total sample volume in the ACSA device, so only a small amount of the large long-term volume variation could occur in this small zone.

Chambon *et al.* (2003) carried out analysis based on a Correlation Image Velocimetry technique (CIV) of the microstructure computed from pictures taken from one of the windows through the ACSA bottom plate. They observed partial strain delocalization during total shear release (corresponding to a reverse offset of about 0.33 10^{-3} m). This delocalization, related to significant displacement of grain clusters, spreads out from the shear band, far away in the bulk of the sample. When shear is resumed, a new localization is promptly reached, and the displacement field out of the shear band becomes negligible. This result suggests that during each shear stress perturbation imposed at the sample/cylinder interface, a perturbation of the displacement field is triggered in the whole sample, initiating a densification. Furthermore, Nakatani (1998) suggested that particle rearrangements during shear release partially destroy the shear localization developed during slip and lead to consolidation restrengthening. The same phenomenon has

been observed by Koval *et al.* (2011) with the ACSA device: after each shear direction reverse, displacement outside of the shear band is very significantly enhanced but return to a long-term value only after a slip of a few grain diameters.

In summary, during shear, the volumetric strain involves mainly the sample bulk outside of the shear band and not the shear band itself which reaches quickly its critical state but is however subjected to long-term comminution. During shear stress perturbations, or shear direction reverse, strain occurs both within and outside of the shear band. Long-term compaction involves the whole sample (with a very small contribution of the shear band), while dilatancy concerns mostly the shear band.

5.5 Implications for fault mechanics

Restrengthening of faults after an earthquake is a key process that controls the seismic cycle. When healing is significant in magnitude, the stress drop of the following earthquake in the cycle might be important. Accordingly it controls also the forthcoming earthquake rupture on the fault. Healing rate has to be compared to loading rate. If the healing rate is fast, the lock time of the fault (or stick period in a stick-slip description) is expected to be increased and the seismic cycle longer. On the contrary, for weak healing compare to loading rate, frequent repeating earthquakes could develop. To understand the physical processes involved during healing, numerous experiments have been performed at laboratory scale (Marone 1998a). The main framework to interpret the results is the description in terms of RSF law (Dieterich 1979b; Scholz 1998). Healing is defined as the increase of the static coefficient of friction with time. It is classically shown to increase logarithmically with time which is interpreted as a creep process that involves plastic deformation at the contact scale. A stimulating debate has emerged when observing that the effective healing rate at laboratory scale was significantly lower than at field scale (Karner *et al.* 1997; Marone 1998b). Our results suggest that healing might be related to a very different process: a time-independent process, as already suggested by Nakatani & Mochizuki (1996) with the 'Tightening-up effect'. In our case, healing is dominated by a mechanical perturbation of the interface, independently of time. The consequence of this observation is that healing might very fast and related to a mechanical perturbation of the surrounding of the fault like distant earthquakes or fault interactions. It can then be proposed as a mechanism involved in static or dynamical triggering. Moreover, the presence of a threshold for the reverse offset to induce healing suggests that triggering might be strongly non-linear.

6 CONCLUSIONS

To investigate the important issue of the mechanical healing of faults, we performed experiments on a simulated fault gouge by the mean of the ACSA. These tests are SRS tests in which an annular sample of sand is sheared up to steady state and then submitted to partial shear stress releases before resuming to initial loading. Shear stress releases are obtained from small reverse offsets of the loading interface. When reverse offsets are sufficiently large, they are shown to induce significant shear strength increase. The reverse offset threshold is of order of 0.05–0.1 10^{-3} m (i.e. a tenth of the grain size). The threshold is expected to be related to a sufficient perturbation of the contact status of the granular assembly. So, we conclude that rather than shear stress perturbations, small reverse offsets are responsible of significant restrengthening of the interface. From large slip experiments (up to 14 m), we show that the material state and attrition effects influence the reverse offset threshold magnitude. As a consequence, large cumulative slip induces a healing strength decrease.

In our experiments, healing is time independent, at least for the adopted release rate. Results show a logarithmic increase, of the healing strength $\Delta\tau_h$ and the induced volumetric strain, both as a function of the reverse offset perturbation $\Delta\delta_c$. We also observed a linear increase of shear strength healing as a function of the induced volumetric strain allowing us to interpret the latter as the main parameter for healing. A small slip perturbation of the loading interface leads to large volumetric compaction that makes the sample denser, and so stronger. This is consistent with the results of Dieterich (1981), Marone & Scholz (1989), Karner & Marone (2001), Nakatani & Mochizuki (1996) and Nakatani (1998), concerning tightening-up or 'Tu effect'.

Finally, we observed that the total volumetric strain is twofold: a continuous slow long-term deformation, and a spontaneous compaction/dilatancy induced by each shear stress perturbation. We suggest that the continuous deformation concerns mainly the bulk of the sample (outside of the shear band) which undergoes very slow compaction, while during shear stress perturbation, the whole thickness of sample is implicated in the rapid and large volumetric strain evolution.

ACKNOWLEDGMENTS

We are extremely grateful to the reviewers who provided very constructive comments which helped to significantly improve the manuscript. We acknowledge S. L. Karner and M. Nakatani for providing their experimental results used in our result analysis. We also acknowledge J. Sulem and M. Nakatani for very fruitful discussions. The project was supported by ANR Grants CATTEL-MODALSIS and RISKNAT-SUPNAF and by INSU (3F program #07CV00).

REFERENCES

Agung, M., Sassa, K., Fukuoka, H. & Wang, G., 2004. Evolution of shear zone structure in undrained ring-shear tests, *Landslides,* **1,** 101–112.

Beeler, N., Tullis, T. & Weeks, J., 1994. The roles of time and displacement in the evolution effect in rock friction, *J. geophys. Res.,* **21,** 1987–1990.

Beeler, N., Tullis, T., Blanpied, M. & Weeks, J., 1996. Frictional behavior of large displacement experimental faults, *J. geophys. Res.,* **101,** 8697–8715.

Chambon, G., 2003. Caractérisation expérimentale du frottement effectif des zones de faille, thèse de l'Université PARIS XI Orsay, France.

Chambon, G., Schmittbuhl, J., Corfdir, A., Vilotte, J. P. & Roux, S., 2003. Shear with comminution of a granular material: microscopic deformations outside the shear band, *Phys. Rev. E,* **68,** 011304, doi:10.1103/PhysRevE.68.011304.

Chambon, G., Schmittbuhl, J. & Corfdir, A., 2006a. Frictional response of a thick gouge sample: a. Mechanical measurements and microstructures, *J. geophys. Res.,* **111,** B09308, doi:10.1029/2003JB002731.

Chambon, G., Schmittbuhl, J. & Corfdir, A., 2006b. Frictional response of a thick gouge sample: b. Friction laws and implications for faults, *J. geophys. Res.,* **111,** B09309, doi:10.1029/2004JB003339.

Chambon, G., Schmittbuhl, J., Corfdir, A., Orellana, N., Diraison, M. & Géraud, Y., 2006c. The thickness of faults: from laboratory experiments to field scale observations, *Tectonophysics,* **426,** 77–94.

Chester, F.M. & Chester, J.S., 1998. Ultracataclasite structure and friction processes of the Punchbowl fault, San Andreas system, California, *Tectonophysics,* **295,** 199–221.

Chester, F.M., Chester, J.S., Kirschner, D.L., Schulz, S.E. & Evans, J.P., 2004. Structure of large-displacement strike-slip fault zones in the brittle

continental crust, in *Rheology and Deformation in the Lithosphere at Continental Margins,* pp. 223–260, Columbia Univ. Press, New York.

Clausen, J.A. & Gabrielsen, R.H., 2002. Parameters that control the development of clay smear at low stress states: an experimental study using ring-shear apparatus, *J. Struct. Geol.,* **24**(10), 1569–1586.

Corfdir, A., Lerat, P. & Vardoulakis, I., 2004. A cylinder shear apparatus, *Geot. Test. J.,* **27**(5), 447–455.

Dieterich, J.H., 1979a. Time-dependent friction in rocks, *J. geophys. Res.,* **77,** 3690–3697.

Dieterich, J.H., 1979b. Modeling of rock friction. 1—experimental results and constitutive equations, *J. geophys. Res.,* **84,** 2161–2168.

Dieterich, J.H., 1981. Constitutive properties of faults with simulated gouge, in *Mechanical Behavior of Crustal Rocks,* Vol. 24, pp. 103–120, eds Carter, N.L., Friedman, M., Logan, J.M. & Stearns, D.W., American Geophysical Union Geophysical Monograph, AGU, Washington, DC.

Garga, V.K. & Sendano, J.I., 2002. Steady state strength of sands in a constant volume ring shear apparatus, *Geotech. Test. J.,* **25**(4), 414–421.

Géminard, J.-C., Losert, W. & Gollub, J.P., 1999. Frictional mechanics of wet granular material, *Phys. Rev. E,* **59**(5), 5881–5890.

Goupy, J., 1993. *Methods for Experimental Design. Principles and Applications for Physicists and Chemists,* Elsevier, Amsterdam.

Karner, S.L., 2006. An extension of rate and state theory to poromechanics, *Geophys. Res. Lett.,* **33**(3), L03308, doi:10.1029/2005GL024934.

Karner, S.L. & Marone, C., 1998. The effect of shear load on frictional healing in simulated fault gouge, *Geophys. Res. Lett.,* **25**(24), 19319–19337.

Karner, S.L. & Marone, C., 2001. Frictional restrengthening in simulated fault gouge: effect of shear load perturbations, *J. geophys. Res.,* **106,** 19 319–19 337.

Karner, S.L., Marone, C. & Evans, B., 1995. Laboratory study of fault healing and lithification in simulated fault gouge under hydrothermal conditions, IUGG 21st General Assembly, Symposium S JS1 Earthquake Generation Processes – Environmental Aspects and Physical Modelling, *Tectonophysics,* **277**(1–3), 41–55.

Karner, S., Marone, C. & Evans, B., 1997. Laboratory study of fault healing and lithification in simulated fault gouge under hydrothermal conditions, *Tectonophysics,* **277,** 41–55.

Koval, G., Chevoir, F., Roux, J.-N., Sulem, J. & Corfdir, A., 2011. Interface roughness effect on slow cyclic annular shear of granular materials, *Granular Matt.,* **13**(5), doi:10.1103/PhysRevE.79.021306.

Lerat, P., 1996. Etude de l'interface sol-structure dans les milieux granulaires à l'aide d'un nouvel appareil de cisaillement annulaire, *PhD thesis,* Ecole Nationale des Ponts et Chaussées, France.

Li, Y.-G., Vidale, J.E., Day, S.M., Oglesby, D.D. & Cochran, E., 1983. Postseismic fault healing on the rupture zone of the 1999 m 7.1 Hector Mine, California, earthquake, *Bull. seism. Soc. Am.,* **93,** 854–869.

Linker, M.F. & Dieterich, J.H., 1992. Effects of variable normal stress on rock friction: observations and constitutive equations, *J. geophys. Res.,* **97**(B4), 4923–4940.

Mair, K. & Marone, C., 1999. Friction of simulated fault gouge for a wide range of velocities and normal stresses, *J. geophys. Res.,* **104,** 28 899–28 914.

Marone, C., 1998a. Laboratory derived friction laws and their application to seismic faulting. Tech. Rep. 26, *Annu. Rev. Earth Planet. Sci.,* 643–696.

Marone, C., 1998b. The effect of loading rate on static friction and the rate of fault healing during the earthquake cycle, *Nature,* **391,** 69–72.

Marone, C. & Scholz, C., 1989. Particle-size distribution and microstructures within simulated fault gouge, *J. Struct. Geol.,* **11,** 799–814.

Marone, C., Vidale, J.E. & Ellsworth, W., 1995. Fault healing inferred from time dependent variations in source properties of repeating earthquakes, *Geophys. Res. Lett.,* **22,** 3095–3098.

Nakatani, M., 1998. A new mechanism of slip weakening and strength recovery of friction associated with the mechanical consolidation of gouge, *J. geophys. Res.,* **103,** 27 239–27 256.

Nakatani, M. & Mochizuki, H., 1996. Effects of shear stress applied to surfaces in stationary contact on rock friction, *Geophys. Res. Lett.,* **23,** 869–872.

Nakatani, M. & Scholz, C., 2004. Frictional healing of quartz gouge under hydrothermal conditions: 1. Experimental evidence for solution transfer healing mechanism, *J. geophys. Res.,* **109,** doi:10.1029/2001JB001522.

Olsen, M.P., Scholz, C.H. & Leger, A., 1998. Healing and sealing of a simulated fault gouge under hydrothermal conditions: implications for fault healing, *J. geophys. Res.,* **103**(B4), 7421–7430.

Richardson, E. & Marone, C., 1999. Effects of normal stress vibrations on frictional healing, *J. geophys. Res.,* **104**(B12), 28 859–28 878.

Ruina, A., 1983. Slip instability and state variable friction laws, *J. geophys. Res.,* **88,** 10 359–10 370.

Scholz, C.H., 1992. *The Mechanics of Earthquakes and Faulting,* Cambridge Univ. Press, New York.

Scholz, C.H., 1998. Earthquakes and friction laws, *Nature,* **391,** 37–42.

Scholz, C.H., 2003. Good tidings, *Nature,* **425,** 670–671.

Sleep, N.H., 1997. Application of a unified rate and state friction theory to the mechanics of fault zones with strain localization, *J. geophys. Res.,* **102**(B2), 2875–2895.

Sleep, N.H., Richardson, E. & Marone, C., 2000. Physics of friction and strain rate localization in synthetic fault gouge, *J. geophys. Res.,* **105,** 25 875–25 890.

Tadokoro, K. & Ando, M., 2002. Evidence for rapid fault healing derived from temporal changes in s wave splitting, *Geophys. Res. Lett.,* **29**(4), doi:10.1029/2001GL013644.

Tika, T.E., 1999. Ring shear tests on a carbonate sandy silt, *Geotech. Testing J.,* **22**(4), 342–355.

Tullis, T.E. & Weeks, J.D., 1986. Constitutive behavior and stability of frictional sliding of granite, *Pure appl. Geophys.,* **124,** 383–414.

Yashuhara, H., Marone, C. & Elsworth, D., 2005. Fault zone restrengthening and frictional healing: the role of pressure solution, *J. geophys. Res.,* **110,** B06310, doi:10.1029/2004JB0033272005.